



Exploring microperimetry and autofluorescence endpoints for monitoring disease progression in *PRPF31*-associated retinopathy

Danial Roshandel , Jennifer A. Thompson , Jason Charng , Dan Zhang , Enid Chelva , Sukanya Arunachalam , Mary S. Attia , Tina M. Lamey , Terri L. McLaren , John N. De Roach , David A. Mackey , Steve D. Wilton , Sue Fletcher , Samuel McLenachan & Fred K. Chen

To cite this article: Danial Roshandel , Jennifer A. Thompson , Jason Charng , Dan Zhang , Enid Chelva , Sukanya Arunachalam , Mary S. Attia , Tina M. Lamey , Terri L. McLaren , John N. De Roach , David A. Mackey , Steve D. Wilton , Sue Fletcher , Samuel McLenachan & Fred K. Chen (2020): Exploring microperimetry and autofluorescence endpoints for monitoring disease progression in *PRPF31*-associated retinopathy, Ophthalmic Genetics, DOI: [10.1080/13816810.2020.1827442](https://doi.org/10.1080/13816810.2020.1827442)

To link to this article: <https://doi.org/10.1080/13816810.2020.1827442>

 View supplementary material 

 Published online: 27 Sep 2020.

 Submit your article to this journal 

 View related articles 

 View Crossmark data 

RESEARCH REPORT



Exploring microperimetry and autofluorescence endpoints for monitoring disease progression in *PRPF31*-associated retinopathy

Danial Roshandel^{a,b}, Jennifer A. Thompson^c, Jason Charny^{a,b}, Dan Zhang^{a,b}, Enid Chelva^c, Sukanya Arunachalam^{a,b}, Mary S. Attia^{a,b}, Tina M. Lamey^{a,c}, Terri L. McLaren^{a,c}, John N. De Roach^{a,c}, David A. Mackey^{a,b,c}, Steve D. Wilton^{d,e}, Sue Fletcher^{d,e}, Samuel McLenachan^{a,b}, and Fred K. Chen^{a,b,c,f,g}

^aCentre for Ophthalmology and Visual Science, The University of Western Australia, Perth, Australia; ^bOcular Tissue Engineering Laboratory, Lions Eye Institute, Nedlands, Australia; ^cAustralian Inherited Retinal Disease Registry and DNA Bank, Department of Medical Technology and Physics, Sir Charles Gairdner Hospital, Nedlands, Australia; ^dCentre for Molecular Medicine and Innovative Therapeutics, Murdoch University, Murdoch, Australia; ^eThe Perron Institute, The University of Western Australia, Nedlands, Australia; ^fDepartment of Ophthalmology, Royal Perth Hospital, Perth, Australia; ^gDepartment of Ophthalmology, Perth Children's Hospital, Nedlands, Australia

ABSTRACT

Background: Mutations in the splicing factor pre-messenger RNA processing factor 31 (*PRPF31*) gene cause autosomal dominant retinitis pigmentosa 11 (RP11) through a haplo-insufficiency mechanism. We describe the phenotype and progression of microperimetry and autofluorescence endpoints in an Indigenous Australian RP11 family.

Patients and Methods: Ophthalmic examination, optical coherence tomography, fundus autofluorescence and microperimetry were performed at baseline and every 6–12 months. Baseline and annual change in best-corrected visual acuity (BCVA), microperimetry mean sensitivity (MS) and number of scotoma loci, residual ellipsoid zone (EZ) span and hyperautofluorescent ring (HAR) area were reported. Next-generation and Sanger sequencing were performed in available members.

Results: 12 affected members from three generations were examined. Mean (SD, range) age at onset of symptoms was 11 (4.5, 4–19) years. MS declined steadily from the third decade and EZ span and HAR area declined rapidly during the second decade. Serial microperimetry showed negligible change in MS over 2–3 years. However, mean EZ span, near-infrared and short-wavelength HAR area reduction was 203 (6.4%) $\mu\text{m}^2/\text{year}$, 1.8 (8.7%) mm^2/year and 1.1 (8.6%) mm^2/year , respectively. Genetic testing was performed on 11 affected and 10 asymptomatic members and *PRPF31* c.1205 C > A (p.Ser402Ter) mutation was detected in all affected and two asymptomatic members (non-penetrant carriers).

Conclusions: Our findings suggest that in the studied cohort, the optimal window for therapeutic intervention is the second decade of life and residual EZ span and HAR area can be considered as efficacy outcome measures. Further studies on larger samples with different *PRPF31* mutations and longer follow-up duration are recommended.

ARTICLE HISTORY

Received July 04, 2020
Revised August 23, 2020
Accepted September 10, 2020

KEYWORDS

Retinitis pigmentosa;
PRPF31; RP11;
non-penetrance; Indigenous
Australian

Introduction

Rapid advances in the treatment of retinitis pigmentosa (RP) have prompted an urgent need for feasible and reliable efficacy outcome measures for use in RP clinical trials (1). Whilst cross-sectional studies may provide data on the feasibility of various clinical tests in RP, a natural history study is necessary to identify the most suitable trial endpoints at various stages of the disease. It is widely recognised that there is significant variation in the natural history between various genetic causes of RP. More recent studies have also shown significant inter- and intra-familial phenotypic variations even amongst patients with the same mutation (2–4). The precursor mRNA processing factor 31 (*PRPF31*)-associated RP (also known as RP11) is one example of this variability in phenotype (5,6).

The precursor messenger RNA splicing factor, *PRPF31*, is encoded by the *PRPF31* gene, which is located on chromosome 19q13.4 (7). Mutations in *PRPF31* are known to cause RP11

and are implicated in up to 10% of autosomal dominant RP (adRP) (8–14). Previous clinical case series of *PRPF31*-associated RP consistently reported phenotypic variations that ranged from non-penetrance to severe early-onset disease (15–18). Age at onset of symptoms varied from early childhood (19) to late adulthood (5) in different families with different mutations. In addition, patients from the same family had different ages at onset of symptoms (5). These observations support the haploinsufficiency hypothesis in which the severity of RP depends on the expression level of the normal *PRPF31* allele inherited from the non-carrier parent (20). Despite the large number of reported cases, there are only two longitudinal studies describing the clinical course of *PRPF31*-associated RP (5,6). Hafler and colleagues studied the annual rate of decline in peripheral visual field area measured by Goldmann perimetry (V4e) and full-field electroretinography (ERG) 30-Hz flicker amplitude in 26 patients with *PRPF31*-associated RP and found 7% and 9% decline per year, respectively (6). The

variability in progression rate was attributed to genetic factors and inter-test variability (6). More recently, Kiser and colleagues reported a comparable annual rate of loss in Goldmann V4e peripheral visual field area (8%) and cone ERG b-wave amplitude (7%) in 26 patients (from 13 families) with *PRPF31* mutations (5). In addition to this functional endpoint, they also reported a 5.4% per year rate of reduction in the area of residual photoreceptor inner segment ellipsoid zone (EZ) in eight unrelated patients (5). However, neither study reported the change in other commonly used endpoint measures in RP trials such as the ring area on fundus autofluorescence (FAF) or microperimetry retinal sensitivity parameters. Both FAF and microperimetry have been shown to reliably map out the preserved central island of vision in RP (21,22). Furthermore, both studies described North American patients with *PRPF31*-associated RP and, to the best of our knowledge, there has been no clinical description of RP or RP11 and its natural history in the Indigenous Australian population.

Herein, we report clinical characteristics and disease progression as measured by functional tests and multimodal imaging in three generations of an Indigenous Australian family with *PRPF31*-associated adRP.

Methods

All individuals in this study were participants in the Australian Inherited Retinal Disease Registry & DNA Bank (AIRDR), a national Registry for IRD research approved by Sir Charles Gairdner Hospital Human Research Ethics Committee (Human Ethics Approval Number 2001–053). These individuals were also monitored for disease progression rate prospectively as participants in the Western Australian Retinal Degeneration (WARD) cohort study, approved by the Human Ethics Committee of the Office of Research Enterprise, The University of Western Australia (RA/4/1/7916). Informed consent was obtained from each participant and these studies were conducted in accordance with the tenets of the Declaration of Helsinki.

Clinical assessment

All available family members underwent comprehensive routine ophthalmic assessment including detailed medical and ocular history, best-corrected distance visual acuity (BCVA), complete slit lamp eye examination, functional assessment and structural multimodal retinal imaging (see below).

A clinical diagnosis of RP was made based on history of impaired night vision, funduscopic findings of attenuated retinal vessels, bone spicules and retinal atrophy, and the observation of a profound reduction in dark-adapted full-field ERG response if available.

Functional endpoint measures

BCVA was measured using the Early Treatment Diabetic Retinopathy Study (ETDRS) chart at 4 and 1 m distance. For patients who were unable to read the ETDRS chart, ability to count fingers, perceive hand motions and perception of light were used to describe visual acuity. Standard 24–2 (52 test loci,

III-white stimulus) automated perimetry was performed using the Humphrey Field Analyzer (HFA-II 750, Carl Zeiss Meditec GmbH, Germany) and visual field mean deviation (MD) values were recorded.

Baseline and follow-up fundus-controlled microperimetry (Macular Integrity Assessment, MAIA, Centervue, Padova, Italy) were performed using the large 10–2 (68 test loci) and the small radial (37 test loci, 37 R) grid patterns to map the retinal sensitivity profile within the macular (central 20° field) and foveal (central 6° field) regions, respectively (Figure S1). Goldman III achromatic stimuli with stimulus duration of 200 ms were presented on a dim white background (1.27 cd/m²) one at a time. The dynamic range of the differential stimulus luminance is 0.08 to 317.04 cd/m², which corresponds to sensitivity values of 36 to 0 dB. Test strategy was 4–2 staircase for both grids. All follow-up testing used the same baseline reference test to ensure registration of same test loci. The average retinal sensitivity of the test grid (mean sensitivity, MS) and the number of loci classified as a dense scotoma (sensitivity <0 dB) or scotoma (sensitivity <25 dB) were recorded. MS and number of loci with scotoma or dense scotoma were used to measure disease progression.

Full-field electroretinography (ERG; RETIport 3.2, Roland Consult, Brandenburg, Germany or in-house custom built) was recorded in accordance with International Society for Clinical Electrophysiology of Vision (ISCEV) standards (23).

Structural endpoint measures

Serial wide-field colour imaging (P200Tx and California, Optos plc, Dunfermline, UK) were performed to document the severity of retinal pigmentation.

Spectral-domain optical coherence tomography (SD-OCT, Spectralis OCT2, Heidelberg Engineering, Heidelberg, Germany) was performed on all patients using a horizontal line scan (100 frames averaged) and a raster volume scan covering the central 30°×25° area (9 frames average per line scan, 61 lines per cube). The foveal-centered horizontal line scans were used for EZ span measurement as described previously (24). Nasal and temporal EZ limits were determined manually by two trained graders (DR and JC) and adjudicated by a retinal specialist (FKC). Automated segmentation of the internal limiting membrane and the Bruch's membrane was performed by the HEYEX software (version 1.9.14.0) and manually adjusted if necessary, particularly in regions affected by epiretinal membrane or retinal pigment epithelial atrophy. The ETDRS mask was manually centered at the foveal dip by visualizing the OCT line scan that cuts through the foveal centre. Total macular volume (TMV) calculated by the HEYEX software were recorded.

Short-wavelength (excitation λ = 488 nm) and near-infrared (excitation λ = 787 nm) fundus autofluorescence (AF, HRA2, Heidelberg Engineering, Heidelberg, Germany) were performed in all patients, capturing the central 30° and 55° of retina. To optimize image quality, the fundus near-infrared reflectance image was set in focus and then refocused inward after switching to the "FA mode" (short-wavelength autofluorescence). This refocus is adjusted according to retinal vessel clarity and 100 frames were averaged to maximize contrast.

Sensitivity was adjusted to avoid over exposure during the averaging process. For near-infrared autofluorescence, the “ICGA mode” (near-infrared autofluorescence) was used and the camera head refocused outward to enhance vessel landmark contrast. The image was optimized after averaging 100 frames whilst balancing between inadequate and too much sensitivity to allow continuous fundus tracking. Both short-wavelength AF (SW-AF) and near-infrared AF (NI-AF) images were examined for the presence of a hyperautofluorescent ring (HAR) and the outer boundaries of this HAR were manually delineated in the 30° images by two trained graders (DR and JC). The maximum horizontal and vertical diameters and the area of the HAR were measured using ImageJ (v1.48, National Institute of Health, USA).

DNA analysis and pathogenicity assessment

DNA samples were sourced, processed and stored as detailed previously (25). DNA from two affected family members was analysed using the next-generation sequencing (NGS) RD SmartPanel (26) version 1 and version 5, respectively, and confirmed by Sanger sequencing (Casey Eye Institute, CEI Molecular Diagnostics Laboratory, Portland, OR, USA). Cascade testing of family members was analysed by Sanger sequencing, performed at CEI, the Australian Genome Research Facility (AGRF; Perth, WA, Australia) or in-house at the Lions Eye Institute using forward (5'-GGGCCTGGTCGCTGA-3') and reverse (3'-GGGGAGGTA CCTGGAGTGG-5') primers. For SmartPanel analysis, all exons and flanking intronic regions were sequenced. Nucleotide one corresponds to the A of the start codon, ATG. The OMIM accession numbers/gene reference sequences utilised are #600138; NM_015629.3.

Variants are described in accordance with Human Genome Variation Society recommendations (27). Pathogenicity was assessed using Mutation Taster (28) with information sought from LOVD, ClinVar, dbSNP, HGMD, Exome Sequencing Project, gnomAD (29), and the scientific literature. Pathogenicity was interpreted in accordance with current guidelines proposed by the American College of Medical Genetics and Genomics and the Association for Molecular Pathology (30), and Jarvik and Browning (31).

Statistical analysis

Data were recorded in Statistical Package for the Social Sciences (SPSS) version 23 (SPSS/IBM, Inc., Chicago, IL, USA). The baseline inter-eye visual acuity difference was less than 15 ETDRS letters in all patients except one patient who had an old traumatic full-thickness macular hole in the left eye. Hence, the right eyes were included in quantitative measurements and statistical analyses. Data distribution was examined visually for normality and data were presented as mean, standard deviation (SD) and range. The annual decay rate of each endpoint measure was calculated using linear regression for each study eye. The mean, SD and range for the slopes for each endpoint measure across subjects were reported. The individual annualized relative changes were calculated as a percentage of the baseline value for each endpoint. A second method for calculating the annual rate of EZ length decline was used by combining dataset across patients. The EZ length was log transformed and plotted against age using data from all subjects with measurements available. Linear regression was performed and the antilog of the gradient was used to derive the overall percentage decline per year for the cohort.

Results

The extended family was divided into three main branches (II:3 is branch A, II:5 is branch B and II:6 is branch C). Twelve affected and six unaffected members were examined with multimodal imaging (Figure 1). Those with disease were invited to return for serial multimodal imaging and automated perimetry at 6–12 monthly intervals as a part of the WARD cohort study (N = 12).

Baseline features in affected family members

Baseline clinical assessment of the 12 available affected members was conducted at a mean (SD, range) age of 31 (13, 14–55) years. Based on self-reported history, the mean (SD, range) age at onset of symptoms was 10.8 (4.5, 4–19) years (Table 1).

BCVA at baseline was hand motion in two patients and the remaining ten had a mean (SD, range) BCVA of 58 (14, 36–75) ETDRS letters (Snellen equivalent of 20/80, 20/200–20/40) in the right eye at a mean (SD) age of 28 (11) years.

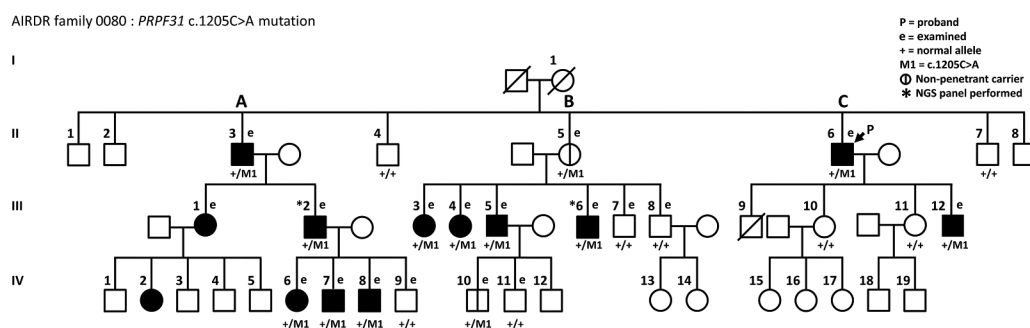


Figure 1. Pedigree of the family showing the autosomal dominant inheritance pattern. Three affected branches of the family are labelled a, b and c. Two non-penetrant carriers (II:5 and IV:10) were found in branch B.

Table 1. Demographic and clinical characteristics of mutation carrying family members (N = 14, including 12 affected and 2 non-penetrant carriers).

ID	Age (y)*	Sex	Onset (y)	FU (y)	BCVA (ETDRS score) [†]		Lens Status		Fundus Features on OCT		
					RE	LE	RE	LE	ODD	CMO	Others
IV:10 [‡]	10	M	NA	1.0	80 (20/25)	75 (20/32)	Clear	Clear			
IV:8	14	M	10	3.3	56 (20/80)	57 (20/80)	Clear	Clear		severe (BE)	
III:12	16	M	12	2.2	69 (20/40)	64 (20/50)	Clear	Clear		severe (BE)	
IV:7	19	M	13	1.8	71 (20/40)	75 (20/32)	Clear	Clear		mild (LE)	
IV:6	21	F	4	0.8	73 (20/40)	70 (20/40)	Clear	Clear		mild (BE)	
III:6	27	M	7	5.2	45 (20/125)	55 (20/80)	mild PSC	mild PSC		mild (BE)	LMD (LE), mild ERM (BE)
III:5	31	M	10	2.7	60 (20/63)	65 (20/50)	mild PSC	Clear	LE		mild ERM (BE)
III:4	31	F	6	5.0	75 (20/32)	75 (20/32)	Clear	Clear			mild ERM (BE)
III:3	33	F	6	5.1	36 (20/200)	50 (20/100)	ASC, PSC	ASC, PSC		mild (BE)	
III:2	38	M	19	1.9	HM	HM	Clear	Clear	BE	mild (RE)	mild ERM (BE)
III:1	42	F	14	0	60 (20/63)	60 (20/63)	Clear	Clear		mild (RE)	LMD (RE), mild (BE)
II:6	50	M	14	5.0	39 (20/160)	HM	mild PSC	mild PSC			TFMH (LE), mild ERM (BE)
II:5 [‡]	54	F	NA	1.5	84 (20/20)	85 (20/20)	Clear	Clear			BRVO (BE)
II:3	55	M	15	4.8	HM	HM	ASC, PSC	ASC, PSC	BE		mild ERM (RE) severe ERM (LE)

*Age at baseline examination. [†]Snellen equivalents are shown in parentheses. [‡]Non-penetrant carrier, asymptomatic.

ASC = anterior subcapsular cataract; BCVA = best-corrected visual acuity; BE = both eyes; BRVO = branch retinal vein occlusion; CMO = cystoid macular oedema; ERM = epiretinal membrane; FU = follow-up duration; HM = hand motion; LE = left eye; LMD = lamellar macular defect; NA = not applicable; OCT = optical coherence tomography; ODD = optic disc drusen; RE = right eye; PSC = posterior subcapsular cataract; TFMH = traumatic full-thickness macular hole.

Five patients (10 eyes) had cataract and two of these underwent bilateral sequential cataract extraction and intraocular lens implantation during the follow-up period. Fundus examination showed variable degrees of intraretinal pigmentation in patients older than 20 years (n = 9). The degree of retinal pigmentation was different in affected family members at similar ages (Figure S2). Optic disc drusen was seen in three family members (II:3, III:2 and III:5) and clinically visible cystoid macula oedema (CMO) was seen in two younger family members (IV:8 and III:12). One patient (II:6) had an old traumatic full-thickness macula hole in the left eye and two patients (III:1 and III:6) had lamellar macular defects (Table 1).

Humphrey visual field (24–2) in ten patients (mean [SD] age = 30 [11] years) showed an average (SD, range) MD of –23.3 (6.6, –14.6 to –33.5) dB. Residual central visual field was present in most patients (Figure S3) and the MD was lowest in the older members of the family (Figure S4). For example, the ranges of MD were –14.6 to –26.8 dB and –20.3 to –33.5 dB in family members aged 18–21 and 35–38 years, respectively (Table S1).

Microperimetry was performed in 10 patients at baseline (Table S1). The large (10–2) test grid (central 20° field) was used in eight patients (mean [SD] age = 28 [12] years). The average (SD, range) MS and the number of scotoma were 10.1 (8.2, 0.0–22.9) dB and 60.8 (9.8, 43–68) loci, respectively. Six (75%) of the eight patients had dense scotoma noted on the 10–2 test; all aged >20 years. The 37 R test (central 6° field) was used in nine patients (mean [SD] age = 31 [11] years). The average (SD, range) microperimetry MS and the number of scotoma were 19.4 (6.8, 6.5–29.2) dB and 25.8 (13.8, 0–37) loci, respectively. Dense scotoma was found in only two of the nine patients (22%), both aged >40 years. Microperimetry MS was lower and the number of scotomatous loci was greater in older family members (Figure 2). Retinal sensitivity was <25 dB in all 10–2 test loci in all patients aged >30 years. The number of scotomatous loci ranged between 0 and 37 in 37 R grid and between 43 and 68 in 10–2 grid.

ERG was performed in only four cases and it demonstrated profound reduction in dark- and light-adapted responses in older affected members while variable residual light-adapted responses were found in the younger members of the family (Figure S5; Table S1).

In addition to the two family members with clinically visible CMO, there were six with intraretinal cysts seen only on OCT. Seven had some degree of bilateral epiretinal membrane on OCT scans with two of these accompanied by lamellar macular defect and one with full-thickness macular hole from trauma (Figure S6). The EZ was clearly visible bilaterally at baseline in six (mean [SD] age = 22 [7] years) of 12 patients (50%), and the mean (SD, range) EZ span was 2932 (1838, 1130–5248) μm (Table S2). The mean (SD, range) TMV was 7.8 (1.4, 6.1–11.1) mm^3 .

A typical HAR was visible in seven (58%) and three (25%) of 12 patients using the NI-AF and SW-AF modality, respectively. The HAR was difficult to detect in those aged >30 years and was absent in all affected family members aged >40 years (Figure 3). In patient IV:8, an irregular HAR was observed in NI-AF while it was not visible in SW-AF image (Figure 3a). Cross-sectional comparison between age-similar affected individuals revealed significant variations in BCVA, MD, MS, EZ span and HAR areas (Table S1 and S2). Eleven affected members returned for follow-up assessment of disease progression rates.

Disease progression in affected family members

Longitudinal BCVA data were available in 11 family members over a mean (SD) interval of 3.4 (1.7) years between the first and the final assessment (Table 2). Although there was an overall decline of BCVA with increasing age across the cohort, it was highly variable in each patient (Figure 4a,b). The mean (SD, range) change in BCVA in nine family members (excluding the two eyes with hand-motion-only vision) was +0.5 (2.4, –2.3 to +5.6) letters per year during follow-up. Neither cataract

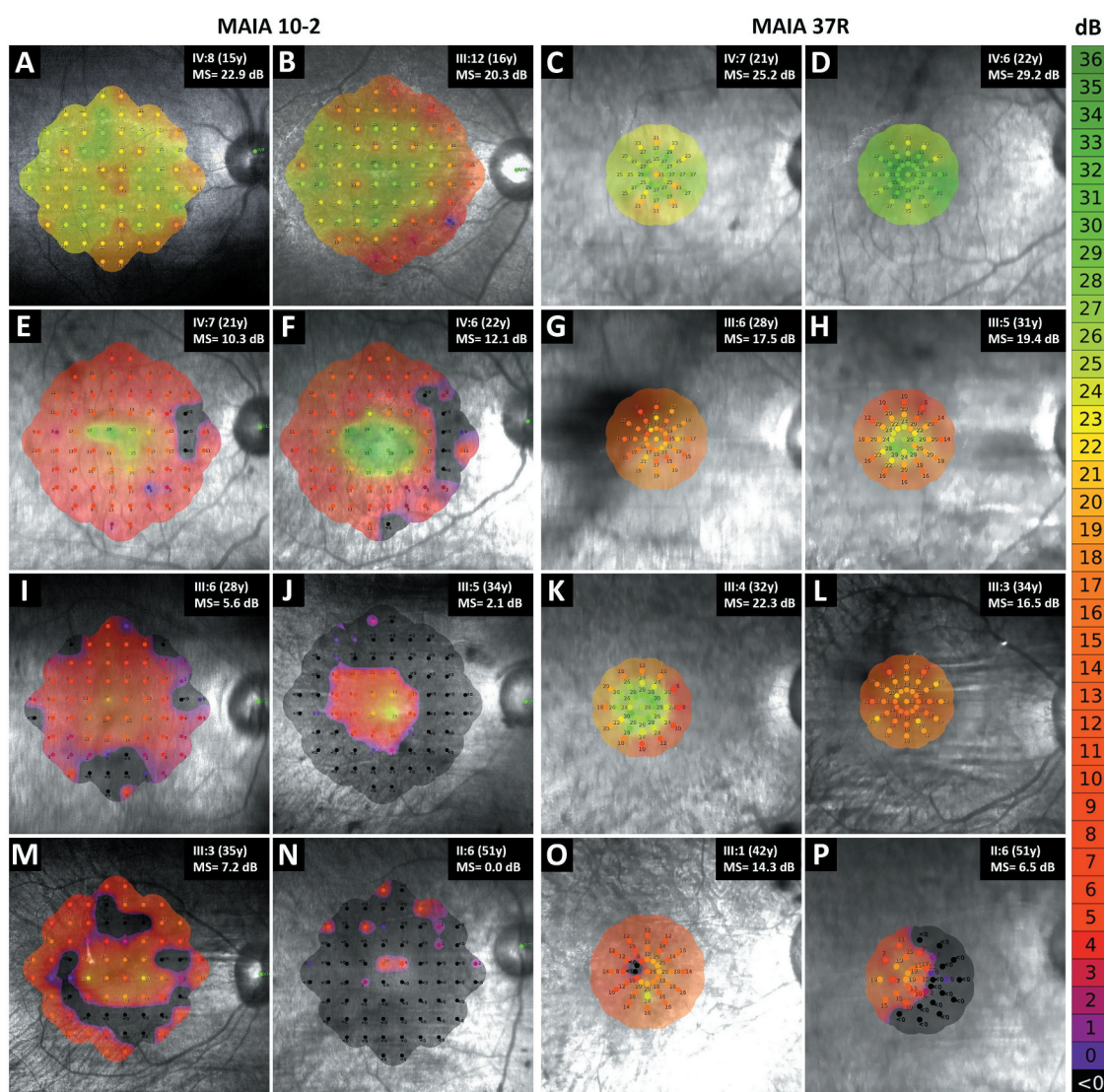


Figure 2. Retinal sensitivity map using 10-2 and 37 R MAIA in affected patients at baseline. Sensitivity scale bar (dB) is shown on the right. Note that dense scotoma (sensitivity below 0 dB) appeared after 20 years in 10-2 grid (e-f) and after 40 years in 37 R grid (O-P) test. MS = mean sensitivity.

surgery (II:3, III:3) nor treating CMO (IV:8, III:12) with oral acetazolamide had any impact on their BCVA.

Serial microperimetry using the large (10-2) test grid (central 20° field) was available in four family members over a mean (SD) follow-up interval of 2.7 (0.6) years (Table 2). The MS and the number of scotomatous loci changed by an average (SD, range) of -0.17 (1.3, -1.8 to $+1.2$) dB and 1.1 (2.0, 0-4.1) loci per year. Five family members had serial microperimetry using the 37 R test (central 6° field) over a mean (SD) follow-up interval of 3.1 (1.0) years (Table 2). The MS and the number of scotomatous loci changed by an average (SD, range) of $+0.10$ (0.9, -1.2 to $+1.1$) dB and $+0.2$ (0.2, 0-0.4) loci per year (Figure 4c-f).

Serial SD-OCT scans were available in 11 affected patients (mean [SD] follow up = 3.4 [1.7] years). In patients without significant CMO or ERM in the right eye ($n = 6$; II:6, III:3, III:4, III:5, IV:6 and IV:7), TMV remained relatively stable during a mean (SD) follow-up period of 3.0 (1.8) years (Figure 5a). In half of all affected family members (12 eyes of six patients), the EZ line was indistinct or absent. Longitudinal data of clearly visible

residual EZ span were available for the remaining six patients (mean [SD] follow up = 2.6 [1.4] years). The mean (SD, range) absolute and relative change in EZ span were -203 (221, -14 to -587) μm and -5.7 (3.7, -1.2 to -11.5) % per year, respectively (Table 3). The most rapid reduction in EZ span was in a 14-year-old subject (IV:8) whilst the most stable was in a 31-year-old subject (III:4) (Table 3 and Figure 5b). An example of EZ change over 26-month in a 16-year-old subject (III:12) is shown in Figure 6. Using log transformation on the combined dataset ($n = 6$, 19 measurements, age range: 14 to 36 years), the estimated rate of change in EZ span was -8.25% and -7.64% in right and left eyes (Figure S7).

Serial NI-AF images also revealed a reduction in HAR horizontal and vertical diameters and area in six patients with longitudinal data (mean [SD] follow-up = 2.5 [1.2] years (Figure 5c-e)). The NI-AF HAR area declined at an average (SD, range) rate of 1.8 (2.7, 0.0 to 6.6) mm^2 or 7.5 (6.7, 0.2 to 16.3) % per year (Table 3). The decline was most rapid during the second decade of life (Figure 5e) and was usually accompanied by severe CMO. Serial SW-AF images showed

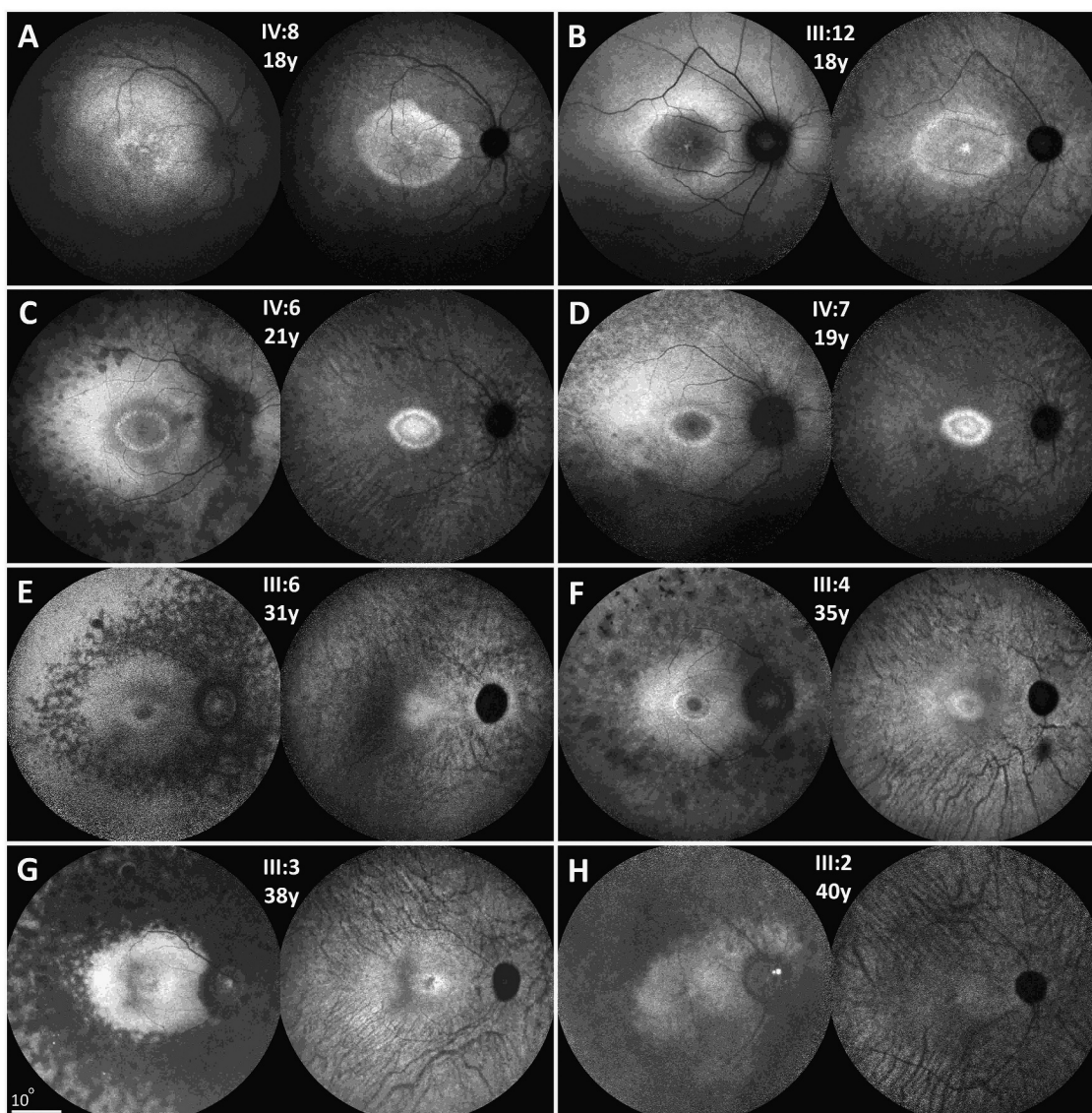


Figure 3. Short-wavelength (left) and near-infrared (right) autofluorescence (AF) patterns of patients at different ages, comparing those at the same age range. Patient IV:8 (a) had a non-specific hyperautofluorescence region on short-wavelength AF imaging and an irregular ring on near-infrared AF imaging. In general, ring structures are easier to visualize on near-infrared excitation.

a reduction in HAR area in three patients with longitudinal data over a mean (SD) follow up of 1.6 (0.7) years. The average (SD, range) decline in SW-AF HAR area was 1.1 (1.2, 0.2 to 2.4) mm² or 8.1 (4.5, 2.9 to 10.7) % per year (Figure 5f; Table 3).

Genetic analysis and pathogenicity assessment

In total, 21 family members (including 11 symptomatic and 10 asymptomatic) contributed DNA and were genetically analysed. A heterozygous nonsense mutation in exon 12 of *PRPF31* (c.1205 C > A; p.Ser402Ter) was detected in the DNA of 13 family members, co-segregating with RP in 11 symptomatic members and displaying non-penetrance in two asymptomatic members (Figure 1). This nonsense variant is considered pathogenic for RP11 due to the premature termination codon and potential for nonsense-mediated decay, absence of the variant from variant databases

including the Exome Sequencing Project and gnomAD (32), and the presence of sufficient informative meioses within the pedigree to substantiate strong evidence of pathogenicity (31). Other variants found using two independent NGS panels in two affected members (III:2 and III:6) were predicted to be either non-pathogenic or non-relevant (Table S3).

Clinical characteristics of non-penetrant cases

Two mutation carriers (aged 10 years; IV:10, and 55 years; II:5) did not have symptoms or signs of RP based on clinical examination by a retina specialist (FKC) and multimodal imaging (Table 1; Figure S8). One non-penetrant case (II:5) had full-field ERG demonstrating normal rod and cone responses (Figure S5). This patient also had bilateral branch retinal vein occlusions without macular involvement.

Table 2. Longitudinal changes in visual acuity and 10–2 and 37 R MAIA mean sensitivity (MS) in affected family members.

ID	Visual acuity (ETDRS score)					MAIA 37 R MS (dB)					MAIA 10–2 MS (dB)							
	Exams (n)	Baseline age (y)	FU (y)	Baseline VA	Slope (letter/y)	Relative change (%)	Exams (n)	Baseline age (y)	FU (y)	Baseline MS	Slope (dB/y)	Relative change (%)	Exams (n)	Baseline age (y)	FU (y)	Baseline MS	Slope (dB/y)	Relative change (%)
IV:8	3	14	3.3	56	-2.3	-4.2	-	-	-	-	-	-	2	15	2.3	22.9	-0.6	-2.7
III:12	5	16	3.0	69	+2.4	+3.5	-	-	-	-	-	-	4	16	2.2	20.3	-1.8	-9.1
IV:7	2	19	1.8	71	-1.1	-1.6	-	-	-	-	-	-	-	-	-	-	-	-
IV:6	2	21	0.8	73	0.0	0.0	-	-	-	-	-	-	-	-	-	-	-	-
III:6	6	27	5.2	45	-0.3	-0.6	5	28	3.8	17.5	+0.1	+0.8	5	28	2.8	5.6	+1.2	+20.7
III:5	3	31	2.7	60	+5.6	+9.4	2	31	2.7	19.4	-1.2	-6.0	-	-	-	-	-	-
III:4	4	31	5.0	75	-1.2	-1.6	3	32	4.0	22.3	-0.1	-0.6	-	-	-	-	-	-
III:3	8	33	5.1	36	+1.0	+2.9	3	34	1.6	16.5	+1.1	+6.9	-	-	-	-	-	-
II:6	8	50	5.0	39	0.0	0.0	5	51	3.4	6.5	+0.6	+8.5	3	51	3.4	0	+0.6	-*
Mean	4.6	26.9	3.5	58.2	+0.5	+0.9	3.6	35.2	3.1	16.4	+0.1	+1.9	3.5	27.5	2.7	12.2	-0.2	+3.0
SD	2.4	11.1	1.6	15.1	2.4	3.9	1.3	9.1	1.0	5.1	0.9	5.9	1.3	16.7	0.7	11.1	1.3	15.7

* Percentage not applicable due to baseline value of 0.

FU = follow-up duration; SD = standard deviation.

Discussion

This is the first detailed description of the clinical course of RP11 in an Indigenous Australian family of 12 penetrant and two non-penetrant members carrying the *PRPF31* c.1205 C > A nonsense mutation. Although there was significant variation in the severity of RP in those of similar ages, the onset of symptoms in all affected members was within the first two decades of life. Standard multimodal imaging and visual field assessment using the Humphrey or MAIA devices were feasible in most patients. There was significant inter-individual variation in progression rates but in general, the most rapid decline occurred during the second decade of life.

Haploinsufficiency and non-penetrance

PRPF31 is the causative gene in up to 10% of adRP cases (11,33). Nearly 90% of *PRPF31* mutations are predicted to result in null alleles (34), supporting haploinsufficiency as the predominant disease mechanism. The nonsense mutation in this pedigree results in the introduction of a premature termination codon (PTC) (p.Ser402Ter) into the *PRPF31* transcript and is predicted to result in haploinsufficiency due to nonsense-mediated mRNA decay (NMD), as has been demonstrated *in vitro* previously for other PTC-encoding *PRPF31* mRNA transcripts (35). Although this mutation was initially reported in a French population (36), the clinical features have not been described.

Incomplete penetrance occurs in the majority of RP11 families reported (33). The rate of non-penetrance was reported between 9–38% in previous studies on different populations (12,18,37,38). Similar to our 10 years old subject (IV:10), there has been a previous report of a non-penetrant *PRPF31* mutation carrier aged 9 years old (5). However, these younger cases may develop symptoms and signs of RP later in their life. Age of onset of symptoms was reported from birth to late adulthood in different families with *PRPF31* mutation (15,19,39), with occasional reports of symptom onset beyond 60 years of age (5). Furthermore, age at onset of symptoms may vary widely (up to 20 years) within the same family (5,39,40), cautioning the clinical diagnosis of non-penetrance in a young asymptomatic carrier. Adding to the clinical dilemma is the lack of consensus regarding the definition of non-penetrance as some papers reported abnormal ERG or dark adaptation in cases that were labeled as non-penetrant (12,38).

Baseline clinical features

Visual acuity in our patients falls within the ranges reported previously in members of families with other *PRPF31* mutations (40–42). Our observation of large variability of visual acuity in patients of similar age has also been reported in other *PRPF31* adRP families (18,37). Factors such as macular oedema, cataract and foveal atrophy due to RP progression are likely to contribute to the variations within the same age group (39,43). Similarly, Humphrey field test showed significant variation in the residual central visual field span and mean deviation irrespective of the patients' age. This was not unexpected given the previous findings in Goldmann visual field test in

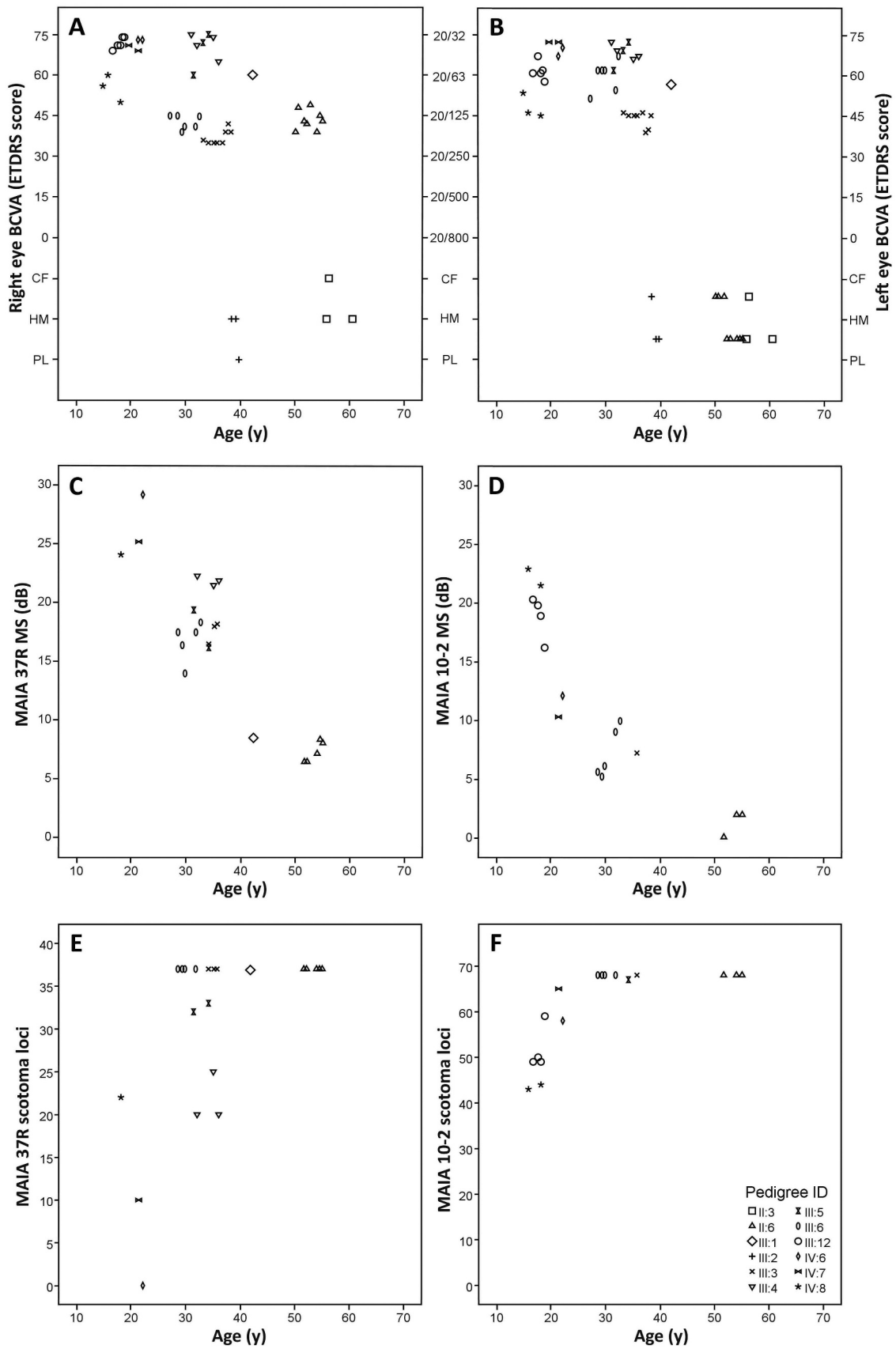


Figure 4. Baseline and follow-up measurements of best-corrected visual acuity (a and b), mean sensitivity (c and d) and number of scotomatous loci (e and f) in affected members. Visual acuity did not change significantly in each patient during the follow up period (a and b). Microperimetry mean sensitivity declined with increasing age across the cohort, which appeared to be linear in 37 R grid (c) and exponential in 10-2 grid (d). The number of scotomatous loci reached a ceiling of 37 in the 37 R grid from the age of 40 years (e). Similarly, the number of scotomatous loci reached a ceiling of 68 in the 10-2 grid from the age of 30 years (f). MS = mean sensitivity. Each symbol represents measurement(s) of one patient as shown in the right-bottom corner.

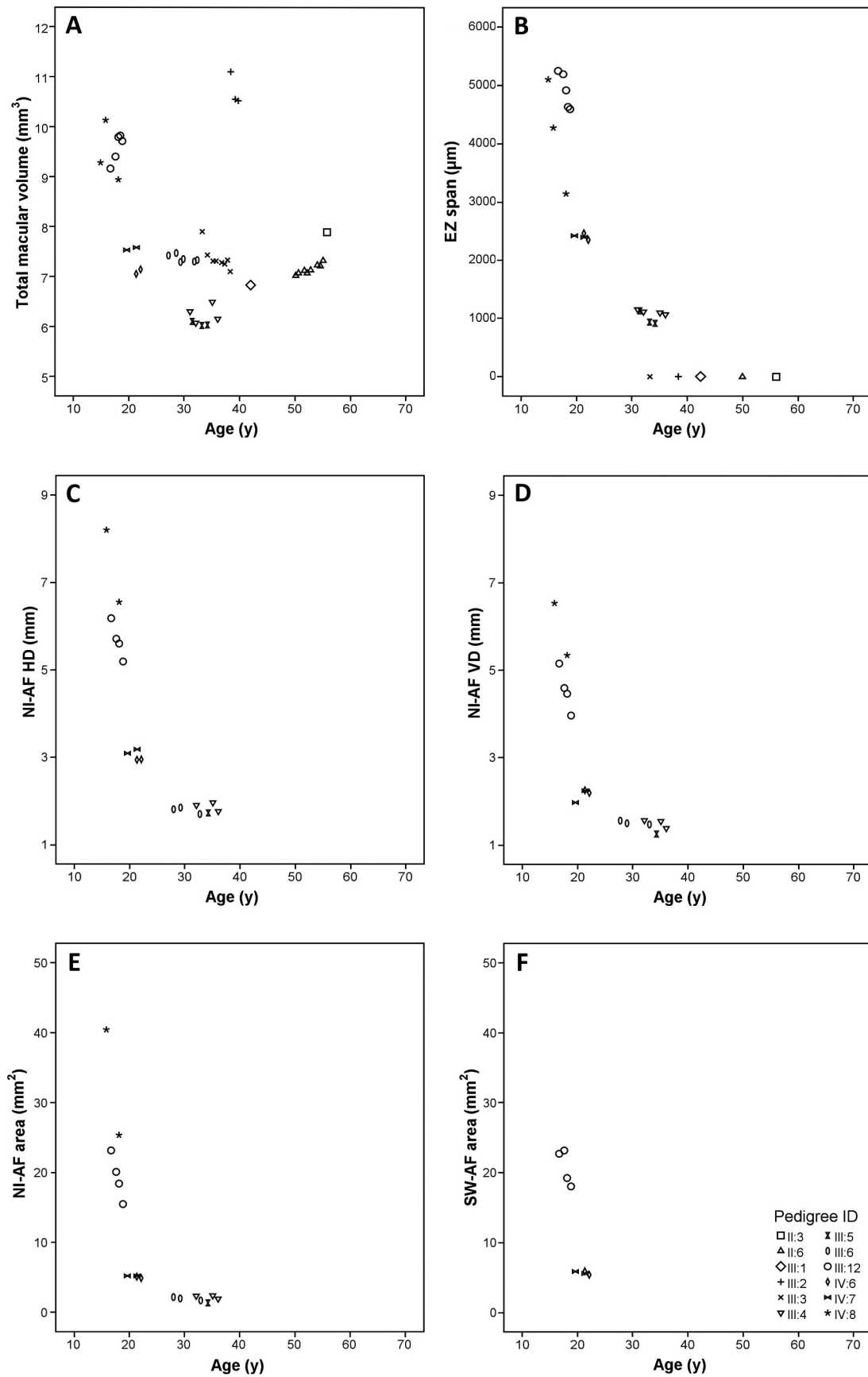


Figure 5. Baseline and follow-up measurement(s) of structural endpoints in affected members. Total macular volume (a) showed high variability, especially in patients with cystoid macular oedema (III:12 and IV:8). Ellipsoid zone (EZ) span (b) and the horizontal diameter (c), vertical diameter (d) and area (e) of the near-infrared autofluorescence (NI-AF) hyperautofluorescent ring appeared to decline exponentially, with the greatest rate in the second decade of life. A similar pattern was observed in short-wavelength autofluorescence (SW-AF) in three patients (f). HD = horizontal diameter; VD = vertical diameter. Plots A-F show structural endpoints versus age in affected members. Each symbol represents measurement(s) of one patient as shown in the right-bottom corner.

Table 3. Longitudinal changes in residual ellipsoid zone span and area of the hyperautofluorescent ring in near-infrared and short-wavelength autofluorescence.

ID	EZ span (μm)					NI-AF HAR area (mm^2)					SW-AF HAR area (mm^2)							
	Exams (n)	Baseline age (y)	FU (y)	Baseline span	Slope ($\mu\text{m}/\text{y}$)	Relative change (%)	Exams (n)	Baseline age (y)	FU (y)	Baseline area	Slope (mm^2/y)	Relative change (%)	Exams (n)	Baseline age (y)	FU (y)	Baseline area	Slope (mm^2/y)	Relative change (%)
IV:8	3	14	3.2	5101	-587	-11.5	2	15	2.3	40.4	-6.6	-16.3	-	-	-	-	-	-
III:12	5	16	2.2	5248	-339	-6.5	4	16	2.2	23.2	-3.5	-15.3	4	16	2.2	22.7	-2.4	-10.7
IV:7	2	19	1.8	2498	-51	-2.1	2	19	1.8	5.2	0.0	-0.2	2	19	1.8	5.9	-0.2	-2.9
IV:6	2	21	0.8	2462	-143	-5.8	2	21	0.8	5.1	-0.3	-4.9	2	21	0.8	5.9	-0.6	-10.7
III:6	-	-	-	-	-	-	3	28	3.7	2.3	-0.1	-4.7	-	-	-	-	-	-
III:5	3	31	2.7	1130	-81	-7.2	-	-	-	-	-	-	-	-	-	-	-	-
III:4	4	31	5.0	1153	-14	-1.2	3	32	4	2.3	-0.1	-3.4	-	-	-	-	-	-
Mean	3.2	22.0	2.6	2932	-203	-5.7	2.7	22.4	2.5	13.1	-1.8	-7.5	2.7	18.7	1.6	11.5	-1.1	-8.1
SD	1.2	7.4	1.4	1838	221	3.7	0.8	6.6	1.2	15.5	2.7	6.7	1.2	2.5	0.7	9.7	1.2	4.5

EZ = ellipsoid zone; FU = follow-up duration; HAR = hyperautofluorescent ring; NI-AF = near-infrared autofluorescence; SD = standard deviation; SW-AF = short-wavelength autofluorescence.

other families with *PRPF31*-associated RP (40,42). Using the MAIA microperimeter, which provides a higher sampling frequency within the central 6°-20° region, we demonstrated the dependence of retinal sensitivity profile on the size of testing grid. Whilst the 10-2 grid mean sensitivity and number of scotomatous loci can be considered as potential markers of disease progression in patients younger than 20-years-old, the 37 R mean sensitivity might be used as a safety endpoint. Of interest, the 10-2 mean sensitivity was not altered by CMO (44), indicating that early stages of CMO, commonly seen in younger patients, may not be an important determinant of macular sensitivity in RP patients. However, since there is no similar report on microperimetry findings in patients with RP11, we recommend further investigation on this potentially useful outcome measure in future RP11 natural history studies.

We noted the frequent occurrence of macular complications such as CMO (predominantly younger members) and ERM (predominantly older members) in SD-OCT, which has previously been reported in other *PRPF31* families (17,18,39,45). The EZ was undetectable in both eyes of five patients (all above 30 years of age) and was ambiguous in all scans of both eyes of a 27-year-old patient (III:6). Nevertheless, preservation of central EZ in patients older than 50 years has been reported in *PRPF31* (5), *USH2A* (4) and *RHO*-associated adRP (46). A HAR may be visible in 58-94% of RP patients using SW-AF imaging (21,47). The occurrence and pattern of the HAR may vary depending on the underlying gene (48) and probably the stage of disease and the imaging modality. Since the boundaries of HAR are compatible with the boundaries of healthy retina in other functional and structural measures (49), it is postulated that the HAR represents the junction between diseased and healthy retina and can be used as a marker of disease progression. Although SW-AF and NI-AF modalities study different molecules within RPE cells (lipofuscin and melanin, respectively), they are highly concordant in dimensions of the detected HAR in RP patients (50). We detected a HAR in 58% and 25% of patients using the NI-AF and SW-AF, respectively. While we did not observe HAR in our patients older than 40 years, there are reports of typical HAR in patients above 50-60 years with other types of RP (4,21,46,51). Based on this observation, we recommend the use of NI-AF rather than SW-AF as a clinical trials endpoint given the higher rate of HAR detection and ease of boundary delineation with NI-AF imaging. The variation in structural and functional outcomes in patients of the same age can be attributed to the expression level of the normal allele (34,43) or, more likely, the inner retinal damage from chronic and untreated CMO.

Natural disease progression

Our longitudinal analysis revealed minimal change in BCVA and microperimetry MS and the number of scotomatous loci in both grids over 2-3 years of follow-up. The rate of BCVA loss in previous studies on *PRPF31* patients was only 0.44%-2% per year (5,6). In addition, visual acuity correlated poorly with age and duration of disease (5). The lack of a measureable progression using MS may be due to the significant test-retest variability of MAIA in retinal diseases (52). There is no report on microperimetry progression in

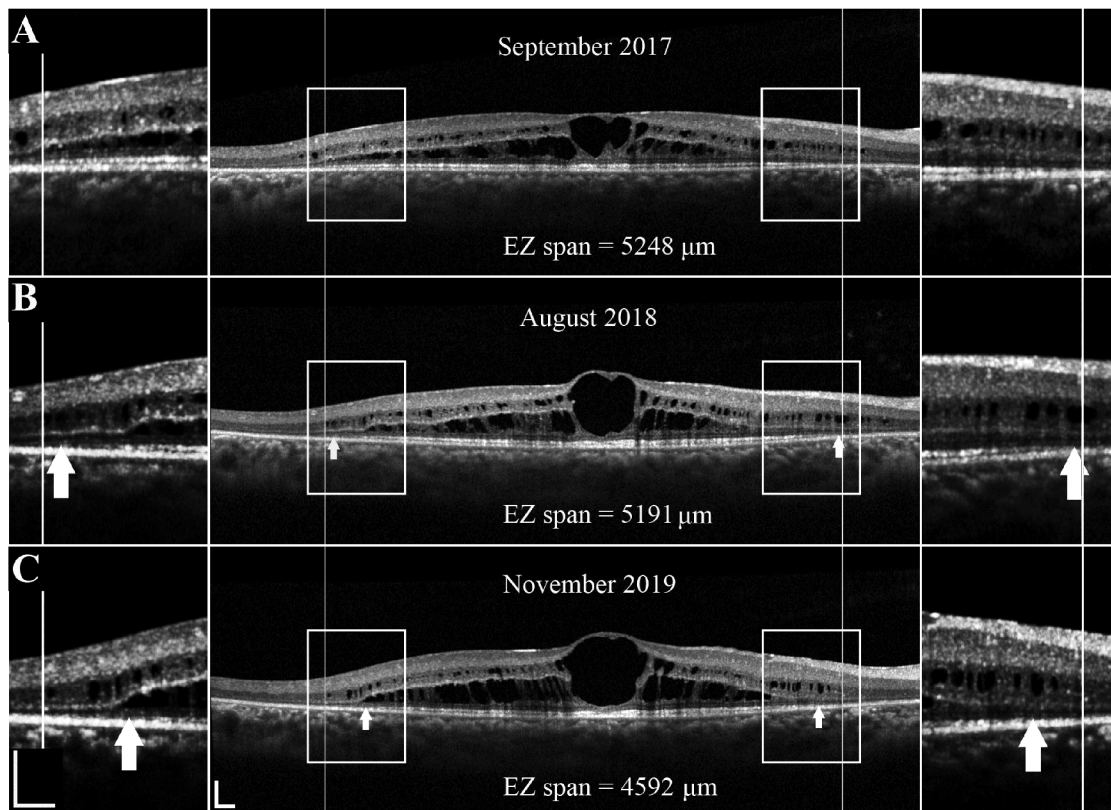


Figure 6. Fovea-centred spectral-domain optical coherence tomography at baseline (a) and after 11 (b) and 26 (c) months in a 16-year-old patient (III:12) shows a 656 μm decrease in the residual ellipsoid zone (EZ) span over the 26-month period. All scans were taken from the same location and aligned vertically. Vertical white lines represent the location of EZ endings at baseline. White arrows show the location of EZ endings on follow-up scans. Magnified views of the transition zone are shown on the left and right side. Scale bars = 200 μm .

PRPF31 patients. Two separate longitudinal studies in unselected RP patients reported a mean and central sensitivity decline of 0.30 and 0.88 dB per year, respectively, using the Nidek MP-1 (53,54). However, these studies did not report the genetic diagnosis in their cohorts. Unlike our microperimetry findings, disease progression has been measured using residual visual field area in Goldmann kinetic perimetry and full-field ERG cone amplitude in two longitudinal studies on *PRPF31*-associated RP. The annual rate of disease progression using these endpoints was 7–8% and 7–9%, respectively (5,6). Based on our results, we recommend a longer follow-up study up to 5 years to measure the decline in macular or foveal MS using trend analysis.

We found a mean reduction of 203 μm per year (an average of 5.7% relative to baseline measure) in the residual EZ span. This loss was greatest in patients aged <20 years (up to 11.5% in one subject). The annual rate of EZ loss in patients with RP has been reported to range from 4.2%–5.2%, which is slightly lower than the rate from pooled data of 7.6% to 8.3% in our cohort (55–57). In the only published report on the longitudinal change of residual EZ in *PRPF31*-associated RP, Kiser and colleagues found a 5.4% per year decline in residual EZ area in 8 patients (5). However, in contrast to our study, their patients had different *PRPF31* mutations and they did not report the mean age and follow-up duration of patients enrolled in their EZ measurement sub-study. In our cohort, the NI-AF and SW-AF HAR area decreased by 7.5% and 8.1% per year, respectively. Longitudinal changes of HAR in

patients with *PRPF31*-associated RP have not been reported. Studies on patients with *RPGR* and *PDE6*-associated RP showed that SW-AF HAR area declines at annual rates of 10.7% and 7.1%, respectively (58,59). There was significant inter-individual and intra-individual variation in the rate of HAR constriction (58,60).

Limitations

Although we reported the detailed structural and functional characteristics including some novel features (i.e. FAF and microperimetry) in a large *PRPF31*-adRP family, our study has several limitations. First, we only reported a relatively small number of patients in the one family. Additional families with other mutations and wild-type *PRPF31* allele expression levels may have different onset age and progression rates. Second, a mean follow-up duration of only 3 years was inadequate for detecting meaningful decline, especially in BCVA and microperimetry parameters. Third, our microperimetry results should be interpreted with caution due to the inherent high variability and we did not specifically estimate the test–retest variability in our patient cohort (52,61). We observed an increase in mean sensitivity in the 6° and 20° test grids in two out of five and one out of four patients, respectively, during the follow-up period. This improvement in retinal function is an indication of the significance of learning effect in masking disease progression and the need for a longer follow-up period to detect

functional decline. Fourth, a large proportion of patients had advanced disease; thus, EZ and HAR could not be measured for disease progression. We did not investigate other methods of structural assessment such as outer nuclear layer thickness and volume measurement in eyes that had lost EZ.

Conclusions

In summary, we described an Indigenous Australian family with the *PRPF31* c.1205 C > A mutation causing adRP, with early onset in those who developed symptoms, and non-penetrance. The affected members showed a rapid structural disease progression in the second decade of life leading to complete loss of EZ and HAR and significant loss of vision by the age of 40. This study supports the value of early rescue treatment in RP11 and provides evidence of intrafamilial phenotypic variation. The optimal window for therapeutic intervention is the second decade of life. Further investigations are needed to explore the role of other genetic and environmental factors in the natural course of *PRPF31*-associated RP and to define the best treatment trial endpoints at various stages of the disease.

Acknowledgments

The AIRDR gratefully acknowledges the assistance from Ling Hoffman and Isabella Urwin of the Department of Medical Technology and Physics, Sir Charles Gairdner Hospital. We also acknowledge the support from Amanda Scurry and Jayme Glynn of Lions Eye Institute in organizing appointment and the transport for the long journeys these patients had to travel for their clinical assessments. We also thank Mr Shang-Chih Chen from the Ocular Tissue Engineering Laboratory for extracting DNA from the biobank for genetic analysis.

Funding

This work was supported by the Australian National Health and Medical Research Council [GNT116360 (DAM, FKC), GNT1188694 (SM, SF, FKC), GNT1054712 (FKC) and MRF1142962 (FKC)], McCusker Foundation (JC), Miocevich Retina Fellowship (MA, SA), Australian Government International Research Training Program Scholarship (DR), and Retina Australia (JAT, TL, JNDR, TLM). The sponsor or funding organization had no role in the design or conduct of this research.

ORCID

Danial Roshandel  <http://orcid.org/0000-0002-6716-6406>
David A. Mackey  <http://orcid.org/0000-0001-7914-4709>

Declaration of interest

FKC: Consultant for PYC Therapeutics, Novartis and Allergan. Other authors have no financial disclosure.

References

- Jacobson SG, Cideciyan AV, Sumaroka A, Roman AJ, Charng J, Lu M, Choi W, Sheplock R, Swider M, Kosyk MS, et al. Outcome measures for clinical trials of leber congenital amaurosis caused by the intronic mutation in the CEP290 gene. *Invest Ophthalmol Vis Sci.* 2017;58(5):2609–22. doi:10.1167/iovs.17-21560.
- Mathijssen IB, Florijn RJ, van den Born LI, Zekveld-Vroon RC, Ten Brink JB, Plomp AS, Baas F, Meijers-Heijboer H, Bergen AA, van Schooneveld MJ. Long-term follow-up of patients with retinitis pigmentosa type 12 caused by *CRB1* mutations: a severe phenotype with considerable interindividual variability. *Retina.* 2017;37(1):161–72. doi:10.1097/iae.0000000000001127.
- Zhang L, Sun Z, Zhao P, Huang L, Xu M, Yang Y, Chen X, Lu F, Zhang X, Wang H, et al. Whole exome sequencing revealed *HKDC1* as a candidate gene associated with autosomal-recessive retinitis pigmentosa. *Hum Mol Genet.* 2018;27:4157–68.
- Calzetti G, Levy RA, Cideciyan AV, Garafalo AV, Roman AJ, Sumaroka A, Charng J, Heon E, Jacobson SG. Efficacy outcome measures for clinical trials of USH2A caused by the common c. 2299delG mutation. *Am J Ophthalmol.* 2018;193:114–29. doi:10.1016/j.ajo.2018.06.017.
- Kiser K, Webb-Jones KD, Bowne SJ, Sullivan LS, Daiger SP, Birch DG. Time course of disease progression of *PRPF31*-mediated retinitis pigmentosa. *Am J Ophthalmol.* 2019;200:76–84. doi:10.1016/j.ajo.2018.12.009.
- Hafner BP, Comander J, Weigel DiFranco C, Place EM, Pierce EA. Course of ocular function in *PRPF31* retinitis pigmentosa. *Semin Ophthalmol.* 2016;31(1–2):49–52. doi:10.3109/08820538.2015.1114856.
- Vithana EN, Abu-Safieh L, Allen MJ, Carey A, Papaioannou M, Chakarova C, Al-Magtheth M, Ebenezer ND, Willis C, Moore AT, et al. A human homolog of yeast pre-mRNA splicing gene, *PRP31*, underlies autosomal dominant retinitis pigmentosa on chromosome 19q13.4 (RP11). *Mol Cell.* 2001;8(2):375–81. doi:10.1016/S1097-2765(01)00305-7.
- Martin-Merida I, Aguilera-Garcia D, Jose PF-S, Blanco-Kelly F, Zurita O, Almoguera B, Garcia-Sandoval B, Avila-Fernandez A, Arteché A, Minguez P, et al. Toward the mutational landscape of autosomal dominant retinitis pigmentosa: a comprehensive analysis of 258 Spanish families. *Invest Ophthalmol Vis Sci.* 2018;59(6):2345–54. doi:10.1167/iovs.18-23854.
- Van Cauwenbergh C, Coppieters F, Roels D, De Jaegere S, Flips H, De Zaeijtj J, Walraedt S, Claes C, Franssen E, Van Camp G, et al. Mutations in splicing factor genes are a major cause of autosomal dominant retinitis pigmentosa in Belgian families. *PLoS One.* 2017;12(1):e0170038. doi:10.1371/journal.pone.0170038.
- Sato H, Wada Y, Itabashi T, Nakamura M, Kawamura M, Tamai M. Mutations in the pre-mRNA splicing gene, *PRPF31*, in Japanese families with autosomal dominant retinitis pigmentosa. *Am J Ophthalmol.* 2005;140(3):537–40. doi:10.1016/j.ajo.2005.02.050.
- Sullivan LS, Bowne SJ, Birch DG, Hughbanks-Wheaton D, Heckenlively JR, Lewis RA, Garcia CA, Ruiz RS, Blanton SH, Northrup H, et al. Prevalence of disease-causing mutations in families with autosomal dominant retinitis pigmentosa: a screen of known genes in 200 families. *Invest Ophthalmol Vis Sci.* 2006;47(7):3052–64. doi:10.1167/iovs.05-1443.
- Bhatia S, Goyal S, Singh IR, Singh D, Vanita V. A novel mutation in the *PRPF31* in a North Indian adRP family with incomplete penetrance. *Doc Ophthalmol.* 2018;137(2):103–19. doi:10.1007/s10633-018-9654-x.
- Bryant L, Lozynska O, Marsh A, Papp TE, van Gorder L, Serrano LW, Gai X, Maguire AM, Aleman TS, Bennett J. Identification of a novel pathogenic missense mutation in *PRPF31* using whole exome sequencing: a case report. *Br J Ophthalmol.* 2018;103:761–67. doi:10.1136/bjophthalmol-2017-311405.
- Wu Z, Zhong M, Li M, Huang H, Liao J, Li A, Guo K, Ma N, Lin J, Duan J, et al. Mutation analysis of pre-mRNA splicing genes in Chinese families with autosomal dominant retinitis pigmentosa. *Curr Mol Med.* 2018;18:287–94.
- Yang Y, Tian D, Lee J, Zeng J, Zhang H, Chen S, Guo H, Xiong Z, Xia K, Hu Z, et al. Clinical and genetic identification of a large Chinese family with autosomal dominant retinitis pigmentosa. *Ophthalmic Genet.* 2015;36(1):64–69. doi:10.3109/13816810.2013.809458.
- Xu F, Sui R, Liang X, Li H, Jiang R, Dong F. Novel *PRPF31* mutations associated with Chinese autosomal dominant retinitis pigmentosa patients. *Mol Vis.* 2012;18:3021–xxx.

17. Evans K, al-Magthteh M, Fitzke FW, Moore AT, Jay M, Inglehearn CF, Arden GB, Bird AC. Bimodal expressivity in dominant retinitis pigmentosa genetically linked to chromosome 19q. *Br J Ophthalmol*. 1995;79(9):841–46. doi:10.1136/bjo.79.9.841.
18. Lu F, Huang L, Lei C, Sha G, Zheng H, Liu X, Yang J, Shi Y, Lin Y, Gong B, et al. A novel PRPF31 mutation in a large Chinese family with autosomal dominant retinitis pigmentosa and macular degeneration. *PLoS One*. 2013;8(11):e78274. doi:10.1371/journal.pone.0078274.
19. Yang L, Yin X, Wu L, Chen N, Zhang H, Li G, Ma Z. Targeted exome capture and sequencing identifies novel PRPF31 mutations in autosomal dominant retinitis pigmentosa in Chinese families. *BMJ Open*. 2013;3(11):e004030. doi:10.1136/bmjopen-2013-004030.
20. Abu-Safieh L, Vithana EN, Mantel I, Holder GE, Pelosini L, Bird AC, Bhattacharya SS. A large deletion in the adRP gene PRPF31: evidence that haploinsufficiency is the cause of disease. *Mol Vis*. 2006;12:384–88.
21. Wakabayashi T, Sawa M, Gomi F, Tsujikawa M. Correlation of fundus autofluorescence with photoreceptor morphology and functional changes in eyes with retinitis pigmentosa. *Acta Ophthalmol*. 2010;88(5):e177–83. doi:10.1111/j.1755-3768.2010.01926.x.
22. Igarashi N, Matsuura M, Hashimoto Y, Hirasawa K, Murata H, Inoue T, Ryo O, Aihara M, Asaoka R. Assessing visual fields in patients with retinitis pigmentosa using a novel microperimeter with eye tracking: the MP-3. *PLoS One*. 2016;11(11):e0166666. doi:10.1371/journal.pone.0166666.
23. McCulloch DL, Marmor MF, Brigell MG, Hamilton R, Holder GE, Tzekov R, Bach M. ISCEV Standard for full-field clinical electroretinography (2015 update). *Doc Ophthalmol*. 2015;130(1):1–12. doi:10.1007/s10633-014-9473-7.
24. Ramachandran R, Cai XC, Lee D, Epstein BC, Locke KG, Birch DG, Hood DC. Reliability of a manual procedure for marking the EZ endpoint location in patients with retinitis pigmentosa. *Transl Vis Sci Technol*. 2016;5(3):6. doi:10.1167/tvst.5.3.6.
25. De Roach JN, McLaren TL, Paterson RL, O'Brien EC, Hoffmann L, Mackey DA, Hewitt AW, Lamey TM. Establishment and evolution of the Australian inherited retinal disease register and DNA bank. *Clin Exp Ophthalmol*. 2013;41(5):476–83. doi:10.1111/ceo.12020.
26. Chiang JP, Lamey T, McLaren T, Thompson JA, Montgomery H, De Roach J. Progress and prospects of next-generation sequencing testing for inherited retinal dystrophy. *Expert Rev Mol Diagn*. 2015;15(10):1269–75. doi:10.1586/14737159.2015.1081057.
27. den Dunnen JT, Antonarakis SE. Mutation nomenclature extensions and suggestions to describe complex mutations: a discussion. *Hum Mutat*. 2000;15(1):7–12. doi:10.1002/(SICI)1098-1004(200001)15:1<7::AID-HUMU4>3.0.CO;2-N.
28. Schwarz JM, Rodelsparger C, Schuelke M, Seelow D. MutationTaster evaluates disease-causing potential of sequence alterations. *Nat Meth*. 2010;7(8):575–76. doi:http://www.nature.com/nmeth/journal/v7/n8/abs/nmeth0810-575.html#supplementary-information.
29. Karczewski KJ, Francioli LC, Tiao G, Cummings BB, Alföldi J, Wang Q, Collins RL, Laricchia KM, Ganna A, Birnbaum DP. Variation across 141,456 human exomes and genomes reveals the spectrum of loss-of-function intolerance across human protein-coding genes. *BioRxiv*. 2019;531210.
30. Richards CS, Bale S, Bellissimo DB, Das S, Grody WW, Hegde MR, Lyon E, Ward BE; Molecular Subcommittee of the ALQAC. ACMG recommendations for standards for interpretation and reporting of sequence variations: revisions 2007. *Genet Med*. 2008;10(4):294–300. doi:10.1097/GIM.0b013e31816b5cae.
31. Jarvik GP, Browning BL. Consideration of cosegregation in the pathogenicity classification of genomic variants. *Am J Hum Genet*. 2016;98(6):1077–81. doi:10.1016/j.ajhg.2016.04.003.
32. Richards S, Aziz N, Bale S, Bick D, Das S, Gastier-Foster J, Grody WW, Hegde M, Lyon E, Spector E, et al. Standards and guidelines for the interpretation of sequence variants: a joint consensus recommendation of the American college of medical genetics and genomics and the association for molecular pathology. *Genet Med*. 2015;17(5):405–24. doi:10.1038/gim.2015.30.
33. Audo I, Bujakowska K, Mohand-Said S, Lancelot ME, Moskova-Doumanova V, Waseem NH, Antonio A, Sahel JA, Bhattacharya SS, Zeitz C. Prevalence and novelty of PRPF31 mutations in French autosomal dominant rod-cone dystrophy patients and a review of published reports. *BMC Med Genet*. 2010;11:145. doi:10.1186/1471-2350-11-145.
34. Rose AM, Bhattacharya SS. Variant haploinsufficiency and phenotypic non-penetrance in PRPF31-associated retinitis pigmentosa. *Clin Genet*. 2016;90(2):118–26. doi:10.1111/cge.12758.
35. Frio TR, Wade NM, Ransijn A, Berson EL, Beckmann JS, Rivolta C. Premature termination codons in PRPF31 cause retinitis pigmentosa via haploinsufficiency due to nonsense-mediated mRNA decay. *J Clin Invest*. 2008;118(4):1519–31. doi:10.1172/JCI34211.
36. Chune V. Apport du séquençage haut débit dans le diagnostic moléculaire de rétinites pigmentaires autosomiques dominantes et liées à l'X: comparaison de quatre stratégies diagnostiques, in Faculte De Medecine. Université Lille 2 Droit Et Santé; 2017.
37. Saini S, Robinson PN, Singh JR, Vanita V. A novel 7 bp deletion in PRPF31 associated with autosomal dominant retinitis pigmentosa with incomplete penetrance in an Indian family. *Exp Eye Res*. 2012;104:82–88. doi:10.1016/j.exer.2012.09.010.
38. Villanueva A, Willer JR, Bryois J, Dermitzakis ET, Katsanis N, Davis EE. Whole exome sequencing of a dominant retinitis pigmentosa family identifies a novel deletion in PRPF31. *Invest Ophthalmol Vis Sci*. 2014;55(4):2121–29. doi:10.1167/iovs.13-13827.
39. Waseem NH, Vaclavik V, Webster A, Jenkins SA, Bird AC, Bhattacharya SS. Mutations in the gene coding for the pre-mRNA splicing factor, PRPF31, in patients with autosomal dominant retinitis pigmentosa. *Invest Ophthalmol Vis Sci*. 2007;48(3):1330–34. doi:10.1167/iovs.06-0963.
40. Lim KP, Yip SP, Cheung SC, Leung KW, Lam ST, To CH. Novel PRPF31 and PRPH2 mutations and co-occurrence of PRPF31 and RHO mutations in Chinese patients with retinitis pigmentosa. *Arch Ophthalmol*. 2009;127(6):784–90. doi:10.1001/archophthalmol.2009.112.
41. Dong B, Chen J, Zhang X, Pan Z, Bai F, Li Y. Two novel PRP31 premessenger ribonucleic acid processing factor 31 homolog mutations including a complex insertion-deletion identified in Chinese families with retinitis pigmentosa. *Mol Vis*. 2013;19:2426–35.
42. Xiao X, Cao Y, Zhang Z, Xu Y, Zheng Y, Chen LJ, Pang CP, Chen H. Novel mutations in PRPF31 causing retinitis pigmentosa identified using whole-exome sequencing. *Invest Ophthalmol Vis Sci*. 2017;58(14):6342–50. doi:10.1167/iovs.17-22952.
43. Utz VM, Beight CD, Marino MJ, Hagstrom SA, Traboulsi EI. Autosomal dominant retinitis pigmentosa secondary to pre-mRNA splicing-factor gene PRPF31 (RP11): review of disease mechanism and report of a family with a novel 3-base pair insertion. *Ophthalmic Genet*. 2013;34(4):183–88. doi:10.3109/13816810.2012.762932.
44. Sayman Muslubas I, Karacorlu M, Arf S, Hocaoglu M, Ersoz MG. Features of the macula and central visual field and fixation pattern in patients with retinitis pigmentosa. *Retina*. 2018;38(2):424–31. doi:10.1097/iae.0000000000001532.
45. Moore AT, Fitzke F, Jay M, Arden GB, Inglehearn CF, Keen TJ, Bhattacharya SS, Bird AC. Autosomal dominant retinitis pigmentosa with apparent incomplete penetrance: a clinical, electrophysiological, psychophysical, and molecular genetic study. *Br J Ophthalmol*. 1993;77(8):473–79. doi:10.1136/bjo.77.8.473.
46. Takahashi VKL, Takiuti JT, Carvalho-Jr JRL, Xu CL, Duong JK, Mahajan VB, Tsang SH. Fundus autofluorescence and ellipsoid zone (EZ) line width can be an outcome measurement in RHO-associated autosomal dominant retinitis pigmentosa. *Graefes Arch Clin Exp Ophthalmol*. 2019;257(4):725–31. doi:10.1007/s00417-018-04234-6.
47. Aizawa S, Mitamura Y, Baba T, Hagiwara A, Ogata K, Yamamoto S. Correlation between visual function and

- photoreceptor inner/outer segment junction in patients with retinitis pigmentosa. *Eye (Lond)*. 2009;23(2):304–08. doi:10.1038/sj.eye.6703076.
48. Trichonas G, Traboulsi EI, Ehlers JP. Correlation of ultra-widefield fundus autofluorescence patterns with the underlying genotype in retinal dystrophies and retinitis pigmentosa. *Ophthalmic Genet*. 2017;38(4):320–24. doi:10.1080/13816810.2016.1227450.
 49. Iriyama A, Yanagi Y. Fundus autofluorescence and retinal structure as determined by spectral domain optical coherence tomography, and retinal function in retinitis pigmentosa. *Graefes Arch Clin Exp Ophthalmol*. 2012;250(3):333–39. doi:10.1007/s00417-011-1823-5.
 50. Duncker T, Tabacaru MR, Lee W, Tsang SH, Sparrow JR, Greenstein VC. Comparison of near-infrared and short-wavelength autofluorescence in retinitis pigmentosa. *Invest Ophthalmol Vis Sci*. 2013;54(1):585–91. doi:10.1167/iovs.12-11176.
 51. Lima LH, Cella W, Greenstein VC, Wang N-K, Busuioc M, Smith RT, Yannuzzi LA, Tsang SH. Structural assessment of hyperautofluorescent ring in patients with retinitis pigmentosa. *Retina*. 2009;29(7):1025–31. doi:10.1097/IAE.0b013e3181ac2418.
 52. Wong EN, Morgan WH, Chen FK. Intersession test-retest variability of 10-2 MAIA microperimetry in fixation-threatening glaucoma. *Clin Ophthalmol*. 2017;11:745–52. doi:10.2147/OPTH.S131371.
 53. Iftikhar M, Usmani B, Sanyal A, Kherani S, Sodhi S, Bagheri S, Schönbach EM, Junaid N, Scholl HPN, Shah SMA. Progression of retinitis pigmentosa on multimodal imaging: the PREP-1 study. *Clin Exp Ophthalmol*. 2019;47(5):605–13. doi:10.1111/ceo.13458.
 54. Chiba A, Miura G, Baba T, Yamamoto S. Determination of length of interdigitation zone by optical coherence tomography and retinal sensitivity by microperimetry and their relationship to progression of retinitis pigmentosa. *Biomed Res Int*. 2019;2019:1217270. doi:10.1155/2019/1217270.
 55. Sujirakul T, Lin MK, Duong J, Wei Y, Lopez-Pintado S, Tsang SH. Multimodal imaging of central retinal disease progression in a 2-year mean follow-up of retinitis pigmentosa. *Am J Ophthalmol*. 2015;160(4):786–98.e4. doi:10.1016/j.ajo.2015.06.032.
 56. Cabral T, Sengillo JD, Duong JK, Justus S, Boudreault K, Schuerch K, Belfort R Jr., Mahajan VB, Sparrow JR, Tsang SH. Retrospective analysis of structural disease progression in retinitis pigmentosa utilizing multimodal imaging. *Sci Rep*. 2017;7(1):10347. doi:10.1038/s41598-017-10473-0.
 57. Colombo L, Montesano G, Sala B, Patelli F, Maltese P, Abeshi A, Bertelli M, Rossetti L. Comparison of 5-year progression of retinitis pigmentosa involving the posterior pole among siblings by means of SD-OCT: a retrospective study. *BMC Ophthalmol*. 2018;18(1):153. doi:10.1186/s12886-018-0817-z.
 58. Tee JLL, Kalitzeos A, Webster AR, Peto T, Michaelides M. Quantitative analysis of hyperautofluorescent rings to characterize the natural history and progression in RPGR-associated retinopathy. *Retina*. 2018;38(12):2401–14. doi:10.1097/iae.0000000000001871.
 59. Takahashi VKL, Takiuti JT, Jauregui R, Lima LH, Tsang SH. Structural disease progression in PDE6-associated autosomal recessive retinitis pigmentosa. *Ophthalmic Genet*. 2018;39(5):610–14. doi:10.1080/13816810.2018.1509354.
 60. Robson AG, Tufail A, Fitzke F, Bird AC, Moore AT, Holder GE, Webster AR. Serial imaging and structure-function correlates of high-density rings of fundus autofluorescence in retinitis pigmentosa. *Retina*. 2011;31(8):1670–79. doi:10.1097/IAE.0b013e318206d155.
 61. Wong EN, De Soyza JDA, Mackey DA, Constable IJ, Chen FK. Intersession test-retest variability of microperimetry in type 2 macular telangiectasia. *Transl Vis Sci Technol*. 2017;6(6):7–7. doi:10.1167/tvst.6.6.7.